E6-2014-1

I. Zvara

VACUUM THERMOCHROMATOGRAPHY: PHYSICAL PRINCIPLES AND MONTE CARLO SIMULATION

Звара И. Е6-2014-1

Вакуумная термохроматография:
физические принципы и Монте-Карло моделирование

Указанный в заголовке метод препаративного разделения следовых количеств относительно летучих элементов или соединений с различной адсорбируемостью основан на молекулярном течении в пустых эвакуированных колонках с наложенным температурным градиентом. Разделяемые вещества, введенные в закрытый горячий конец трубки, начинают мигрировать благодаря случайным полетам молекул между двумя последовательными ударами в стенку. Каждое столкновение сопровождается адсорбцией и некоторым случайным временем пребывания молекулы на поверхности, которое в среднем растет по ходу. В результате различные вещества практически останавливают свое движение в индивидуальных температурных интервалах. Микроскопическая картина молекулярных историй здесь описывается количественно и в деталях, в предположении, что угловое распределение векторов скоростей десорбирующихся молекул определяется законом косинуса. Выведены функции плотности вероятностей для полных свободных пробегов и их проекций для длинных цилиндров. Они использовались для моделирования большого числа историй, чтобы получить профили зон. Моделировались многочисленные частные наборы режимов и условий опытов, чтобы выявить влияние этих параметров на профили зон и на характерные температуры осаждения.

Работа выполнена в Лаборатории ядерных реакций им. Г. Н. Флерова ОИЯИ.

Сообщение Объединенного института ядерных исследований. Дубна, 2014

Zvara I. E6-2014-1

Vacuum Thermochromatography:
Physical Principles and Monte Carlo Simulation

The title method for preparative separation of infinitesimal amounts of relatively volatile elements or compounds with different adsorbability is based on the molecular flow in an evacuated open column with imposed temperature gradient. The analytes put into the column's closed "hot" end begin to migrate owing to random flights of their molecules between two consecutive collisions with the wall. Each strike results in adsorption of the entity on the surface for a random time whose mean increases "downstream"; as a result, various analytes come to practical rest in individual temperature ranges. Here, the microscopic picture of the molecular histories is described in quantitative details, assuming that the velocity vectors of the desorbing molecules obey the cosine law angular distribution. The probability density functions for the full and projected flight lengths in long cylinders are derived. They were used in Monte Carlo simulation of great many migration histories to obtain the peaking profiles of the deposits. Numerous particular sets of experimental regimes and conditions were simulated to elucidate influence of these variables on the profiles and the characteristic deposition temperatures.

The investigation has been performed at the Flerov Laboratory of Nuclear Reactions, JINR.

Communication of the Joint Institute for Nuclear Research. Dubna, 2014

INTRODUCTION

The fundamental processes behind the well-known *gas–solid thermochromatography (GTC)* are: temperature-dependent *reversible adsorption* of the molecules or atoms on the column surface; their transportation down the column by the *convective flow* of a practically *nonadsorbable gas*; and the negative downstream *temperature gradient* along the column. Due to the latter, the speed of migration of the analytes steadily decreases downstream. When, after some time of processing, the column is "frozen" well below the working temperature to stop the migration, the deposits of various analytes are found peaking at individual distances from the origin. To date, the GTC-based techniques have shown to be efficient tools for studying chemical properties of the transactinoid elements, whose isotopes are mostly short-lived and are available only on one-atom-at-a-time scale. For the purpose, the newborn atoms recoiling from a target bombarded by accelerated heavy ions are stopped in the flowing gas. If necessary, it contains also some chemically active agents as well as minute amounts of "carriers" — the compounds which are chemically similar to (or identical with) the radiolabeled entities under study. Such scheme provided yet unsurpassed rate of synthesis and separation of relatively volatile compounds, because in certain experimental conditions, it is possible to register the alpha or spontaneous fission decay events in real time and with high efficiency.

Here we consider a very different situation: *infinitesimal amounts* of several analytes are placed into the closed hot end of an open thermochromatographic column, which is so highly evacuated that any atoms or molecules migrate only by the truly *molecular flow*. In spite of the absence of any downstream viscous flow, sudden freezing of the column after some time of processing reveals separated peaking deposits, which resemble the outcome of GTC experiments. This is why the method is called *vacuum thermochromatography* (VTC). The present paper is continuation of our work [1]; here we provide more details of the fundamentals of VTC and a deeper insight into the migration histories to make possibly rigorous Monte Carlo (MC) simulation of the VTC peaks profiles — their shapes and positions.

First, let us consider an open evacuated isothermal tube, much longer than its diameter, whose surface is uniform in adsorption and other physicochemical

properties. The molecules migrate along the column through erratic free flights between consecutive collisions with the walls. The true molecular flow regime implies that the molecules under study do not collide mutually or with the residual gas along their total path in the experiment. For the millimeter order column diameters and, typically, several hundreds of free flights (see the data later below) it means a total pressure of less than 10^{-4} mmHg (0.01 Pa). Steckelmacher [2] thoroughly reviewed the historical and modern quantitative studies of various aspects of the flow for the case of the *nonadsorbable* molecules, which spend all their time in flights. Meanwhile, when a *moderately adsorbable* molecule strikes the surface, it gets adsorbed and spends some time in this state [3, 4]. The mean of this sojourn is proportional to the inverse Boltzmann exponential factor and so strongly increases with lower temperature. In the here considered experimental conditions, the molecules spend much more time on the surface than in the flights. Hence, the running-time-dependent profile of the original adsorbed fraction practically does not differ from the distribution in the quickly frozen column.

Provided that the flights are reflected at the start point, the profile obtained in the isothermal column must be close to the half-normal distribution [5]. As such, it keeps the maximum value at the zero coordinate and steadily widens with the duration of the experiment. Away from the start, there cannot appear any maximum in the deposit density, and different species yield similar profiles with just unequal spread. However, if the column temperature decreases with distance from the hot end, the analytes deposit as more or less separated peaks. It happens because ever more molecules reach the coordinates (temperatures) at which they fail to rebound during the remaining time. Thus, the lower flight frequency at lower temperature produces a seeming mass flow towards the cold end of the column, and the analytes with different desorption energies yield peaks at different positions. The technique was pioneered by Westgaard et al. [6], first separations were done in the 1970s [7-9]. More works related to the problems considered in the present paper were published only relatively recently [10-12]. The experimental data like the temperature at the mean coordinate of the peak may serve to evaluate desorption energies provided that there is a detailed theory of the processes in the columns.

The simple microscopic picture of the migration calls for Monte Carlo (MC) simulations. Davis [13] seems to have performed the first such simulations, aiming to serve practical purposes. For the citations of more recent studies and for the state of art see [14]. These works concerned the behavior of *nonadsorbable* molecules in isothermal ducts of various configurations to estimate the evacuation rate or the vacuum conductance of complex ducts. The total sojourn time in the duct was obtained from the total path length of the molecules.

When simulating VTC, one follows the histories of *adsorbable* molecules, and of major concern is the total time spent in the adsorption state, because that

spent in the flights is mostly negligible [1]. Our first goal was to elucidate how the experimental parameters affect the shape and position of the VTC peaks. To date, only a few works have reported empirical fitting of the experimental histograms by MC simulations. Their authors considered both the thermal gradient [11, 12] and isothermal [12] columns. In [12], they also measured and simulated the percentage of radioactive nuclides surviving at the column exit, rather than the chromatograms. Their experimental parameters were the time of the experiment and the column temperature, while the desorption energy was an adjustable parameter. Some details of the simulations were published only later [15]. We found that these works contain errors [16], and so here we carefully discuss the background and realization of the correct MC procedures.

We present the simulated vacuum thermochromatograms for numerous combinations of the experimental parameters. The sample graphs were obtained for the conditions envisaged in the chemical studies of the heaviest presently known elements. Basically, the conditions are characterized: by the columns' geometry and temperature regime; by the molecular properties and adsorption characteristics of the analytes; as well as by the individual times of experiment of each single entity. The latter situation takes place especially when the radioactive "label" of the analyte has the mean lifetime much shorter than the nominal duration of the experiment and the coordinate of each decay event is registered in real time.

MICROSCOPIC PICTURE OF MOLECULAR MIGRATIONS

Simulation of the molecular flow in ducts requires knowledge of the angular distribution of the velocity vectors of desorbing molecules. In the spherical coordinates, the differential solid angle is $d\Omega = d\varphi\, d\theta \sin\theta$ and for the "isotropic distribution", the amount of flux is just proportional to $d\Omega$. However, the rebounding molecules must obey the *Knudsen cosine law*, when the flux varies like $\cos\theta d\Omega$. Direct measurements of this distribution are difficult and scarce; however, there are enough fundamental arguments in favor of the law. Some come from fundamental thermodynamics [2, 17, 18]; revision of the molecular diffusion in the terms of a complex dynamical reflection [19] evidences an asymptotic nature of the cosine law on the atomic scale; and a billiard ball model of collisions with wall shows that the law must hold even at the zero adsorption time [20]. The distribution is characteristic of the emission of nuclear radiation and so must be taken into account when the experimental data consist in the real time registration of α particles or spontaneous fission fragments.

The first problems solved here are the probability density functions for the free flight lengths and their projection on the column axis. The adsorption site is taken as the origin of both the spherical and Cartesian coordinates; see Fig. 1.

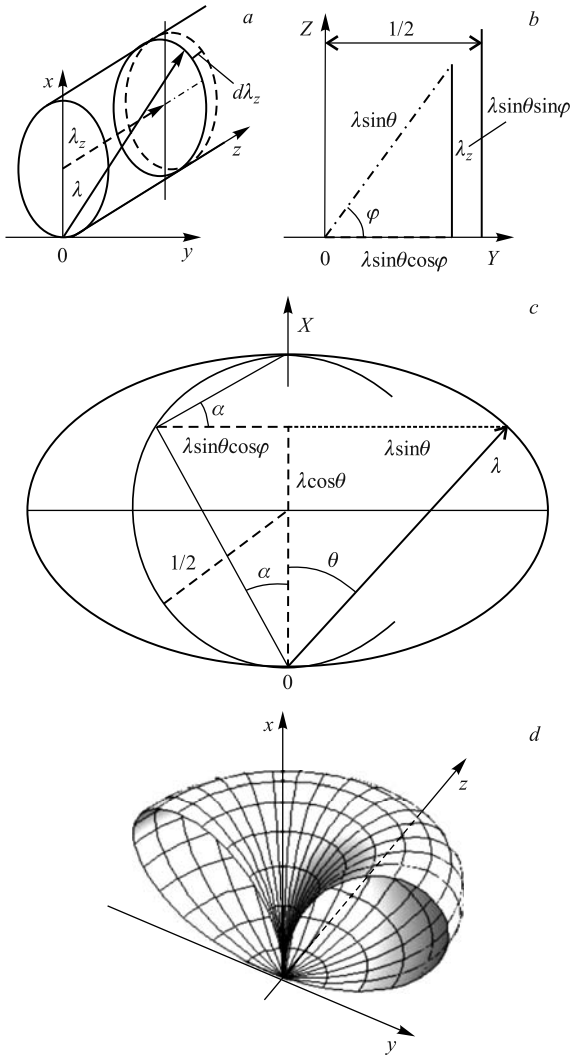

Fig. 1. Geometry of a free flight in the cylindrical column of unit diameter and the cosine-law angular distribution. a) 3D view of the flight and its projection on the tube axis; $d\lambda_z$ is the differential projection length. b) Projections of the involved quantities on the $y-z$ plane. c) Section of the cylinder by the plane defined by x-axis and the flight vector (cf. b); the ancillary left side shows additional geometrical relations; sections b) and c) are to scale with each other. d) 3-D graph of the cosine law distribution of the rebound vectors

The x-axis is perpendicular to the surface, so to the $z-y$ plane, while the cylinder extends along the z-axis. Instead of considering the true length of the flight l and its projection on the z-axis l_z, one may measure them in the cylinder diameters d_c to obtain some universal "reduced" quantities $\lambda \equiv l/d_c$ and $\lambda_z \equiv l_z/d_c$. For the spherical coordinates, we denote by θ the polar angle of the flight vector with the x-axis and by φ — the angle between the projection of the vector on the $y-z$ plane.

Figure 1, *c* helps to find the formula for the free flight length as a function of the angular coordinates. As $\mathrm{tg}\alpha = \mathrm{tg}\theta\cos\varphi$, the reduced lengths depend on the angles like

$$\lambda = \frac{\cos\theta}{1-\sin^2\theta\sin^2\varphi} \tag{1}$$

and

$$\lambda_z = \frac{\cos\theta\sin\theta\sin\varphi}{1-\sin^2\theta\sin^2\varphi}. \tag{2}$$

Their means are obtained by double integration in the range [0, $\pi/2$] for both θ and φ, i. e., in a solid angle of $\pi/2$. The normalizing factor for the cosine distributions comes from

$$\int_0^{\pi/2}\int_0^{\pi/2} \cos\theta\sin\theta d\varphi d\theta = \frac{\pi}{4} \tag{3}$$

so that

$$\overline{\lambda} = \frac{4}{\pi}\int_0^{\pi/2}\int_0^{\pi/2} \frac{\cos\theta}{1-\sin^2\theta\sin^2\varphi}\cos\theta\sin\theta\, d\varphi\, d\theta = 1 \tag{4}$$

and

$$\overline{\lambda} = \frac{4}{\pi}\int_0^{\pi/2}\int_0^{\pi/2} \frac{\cos\theta\sin\theta\sin\varphi}{1-\sin^2\theta\sin^2\varphi}\cos\theta\sin\theta\, d\varphi\, d\theta = \frac{1}{2}. \tag{5}$$

The second moments of the distributions are obtained similarly. Table 1 summarizes the corresponding data. Figure 1, *d* shows that the relatively long flights are suppressed because they happen only if, simultaneously, $\varphi \to \pi/2$ and $\theta \to \pi/2$.

Of much interest are the probability density functions (PDF) and cumulative probability distribution functions (CPDF) of various quantities x; these are denoted below by $\rho(x)$ and $\Pi(x)$, respectively. To our best knowledge, the PDFs of full and projected flights in the above specific geometrical conditions have not yet been considered in literature. Help comes from some works on the geometrical

Table 1. Statistical characteristics of the flight length distributions for the cosine law

First moments		Second moments		Dispersions	
$\bar{\lambda}$	$\bar{\lambda}_z$	$\overline{\lambda^2}$	$\overline{\lambda_z^2}$	σ^2	σ_z^2
1.00*	0.50	1.333	0.666	0.333	0.416

* The value 1.386 reported by the present author earlier [22] was in error.

efficiencies of nuclear radiation detectors; they contain formulas for the solid angle subtended by a circle. Figure 1 *a, b* shows that the present case is a particular one — the emission point lies on the generatrix of the right circular cylinder, at a distance $\lambda_z$from its base. However, only Prata [21] seems to have solved the problem of the solid angle $\Omega(\lambda_z)$, when the source and circle axes are mutually orthogonal and the emission follows the cosine law. He obtained

$$\Omega(\lambda_z) = \pi \left(\frac{2\lambda_z^2 + 1}{2\sqrt{\lambda_z^2 + 1}} - \lambda_z \right). \tag{6}$$

In our case of open cylinder, $\Omega(\lambda_z)$ obviously equals the solid angle subtended by the tube surface from the distance λ_z to infinity. Figure 1, *a* shows that the fraction of the rebounding molecules striking a circular ring with the width $d\lambda_z$ is proportional to the differential change in the solid angle: $\rho(\lambda_z)d\lambda_z \propto -d\Omega(\lambda_z)$. Hence, $\Pi(\lambda_z)$ and $\rho(\lambda_z)$ are related as

$$\Pi(\lambda_z) = 1 - \frac{\Omega(\lambda_z)}{\pi} \quad \text{and} \quad \rho(\lambda_z) \equiv \frac{d}{d\lambda_z}\Pi(\lambda_z) = -\frac{d}{d\lambda_z}\frac{\Omega(\lambda_z)}{\pi}. \tag{7}$$

Then, the CPDF is

$$\Pi(\lambda_z) = 1 - \left(\frac{2\lambda_z^2+1}{\sqrt{\lambda_z^2+1}} - 2\lambda_z \right) \tag{8}$$

and the PDF is

$$\rho(\lambda_z) = 2 - \frac{3\lambda_z + 2\lambda_z^3}{(1+\lambda_z^2)^{3/2}}. \tag{9}$$

The latter rather rapidly decreases with the walk length:

$$\rho(\lambda_z) \underset{\lambda_z \to \infty}{\approx} \frac{3}{4\lambda_z^4} + O\left(\frac{1}{\lambda_z^5}\right). \tag{10}$$

The distributions are displayed in Fig. 2.

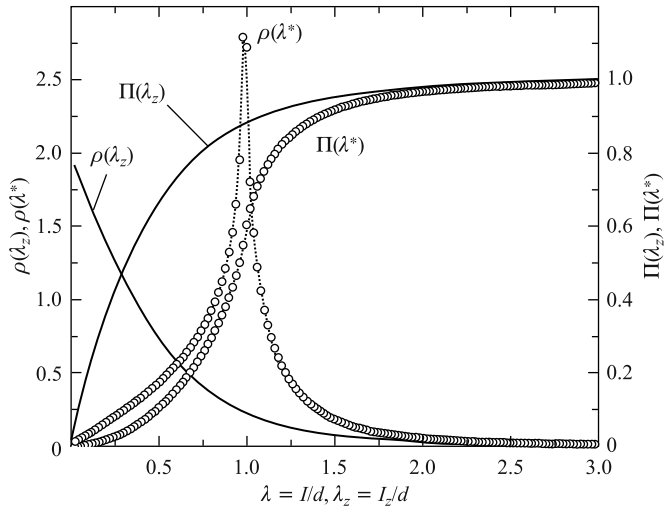

Fig. 2. Solid curves: PDF and CPDF of the projected flights according to Eqs. (8) and (9). Symbol curves: the distributions of full flight lengths obtained by MC simulations (see below)

MONTE CARLO SIMULATION OF THE CHROMATOGRAMS

Free Flights. When the analytic formulas for the above-considered PDFs or CPDFs could not be derived, we made the appropriate MC simulations. Necessarily, these yield the distributions as histograms. Here and below, we denote by x^* a random value of the quantity x and by $\rho(x^*)$ and $\Pi(x^*)$ — the appropriate distributions, to emphasize their MC origin. The PDFs of θ and φ belong to the class, for which the random x^*'s can be obtained [22,23] as the solution of

$$\xi = \Pi(x^*) \equiv \int_0^{x^*} \rho(x)dx, \tag{11}$$

where ξ is a random number from the standard uniform distribution.

When simulating the PDF and CPDF of the length of free flights, the values of λ^* and λ_z^* are calculated from Eqs. (1) and (2), respectively. The required random azimuthal and polar angles in the range $[0, \pi/2]$ are

$$\varphi^* = \frac{\pi}{2}\xi \tag{12}$$

and

$$\theta^* = \arcsin\sqrt{\xi} \tag{13}$$

because $\xi = 2\int_0^{\theta^*} \sin\theta\cos\theta\, d\theta = \sin^2\theta^*$. Alternatively, Eq. (8) provides the direct way to obtain the absolute values of λ_z^* as the algebraic solution of the equation $\xi = \Pi(\lambda_z^*)$, cf. Eq. (11). It gives *

$$\lambda_z^* = \frac{1}{12(\xi-1)}\left[1-2\xi+\xi^2+\frac{(\xi-1)^2(-47-2\xi+\xi^2)}{\psi(\xi)}+\psi(\xi)\right], \qquad (14)$$

where

$$\psi(\xi) = \big[-71-150\xi+663\xi^2-596\xi^3+159\xi^4-6\xi^5+\xi^6+ \\ +12\sqrt{3}\sqrt{(-1+\xi)^4(3-2\xi+\xi^2)^2(28-2\xi+\xi^2)}\big]^{\frac{1}{3}}.$$

Because such a formula could be found only for λ_z^*, all the VTC — related simulations below were consistently done using random angular coordinates. Up to 10^6 flights were simulated for each of the required PDFs and CPDFs in Fig. 2 to obtain histograms with the bins 0.02. We also simulated the distributions with known formulas to check that the histograms (not shown in Fig. 2) closely follow the curves. Notice the striking differences in the distributions of the free flight lengths and their projections.

Flow Chart for VTC Peaks. We shall denote the true, yet unknown PDF of the migration distances by $\rho(z)(\mathrm{cm}^{-1})$. Formation of the VTC peaks proceeds through the (one–dimensional) *random walks with variable steps* and each step is followed by an exponentially distributed time break, whose mean depends on the running coordinate. The chain stops when the accumulated retention time exceeds a preset value, which happens after very different numbers of steps. Our MC simulation flow chart is shown in Fig 3. The accepted symbols (and dimensions) for the quantities and variables encountered in the flow chart are

ε_d–desorption energy per molecule or mole,
ε–desorption energy divided by the universal gas constant (K),
g–local temperature gradient along the column (K cm^{-1}),
T_S–temperature of the hot (start) end of the column (K),
z–distance from the start (cm),
T_z–local column temperature at the distance z (K),
t_e–nominal duration of the experiment (s),
t_lt–mean lifetime of the radionuclide (s),
t_lt^*–random individual lifetime of the label (s),
$\bar{\tau}_a = \bar{\tau}_a(T_z)$–mean adsorption sojourn time (s).

Notice that $t_\mathrm{lt}^* = -t_\mathrm{lt}\ln\xi$ and $\tau_a^* = -\bar{\tau}_a\ln\xi$.

*Obtained using Mathematica7, Wolfram Research Inc.

We made the simulations on some important *assumptions*. First, that the column surface is absolutely homogeneous and has a regular atomic structure with distinct adsorption sites, which are characterized by a single $\varepsilon_{\rm d}$. Next, that the mean adsorption time is $\bar{\tau}_a = \tau_0 e^{\varepsilon/T_z}$, while τ_0, the inverse vibration frequency of the adsorbed entity, does not depend on temperature. We considered the columns with stationary, linear temperature profiles $T_z = T_{\rm S} - {\rm g}z$.

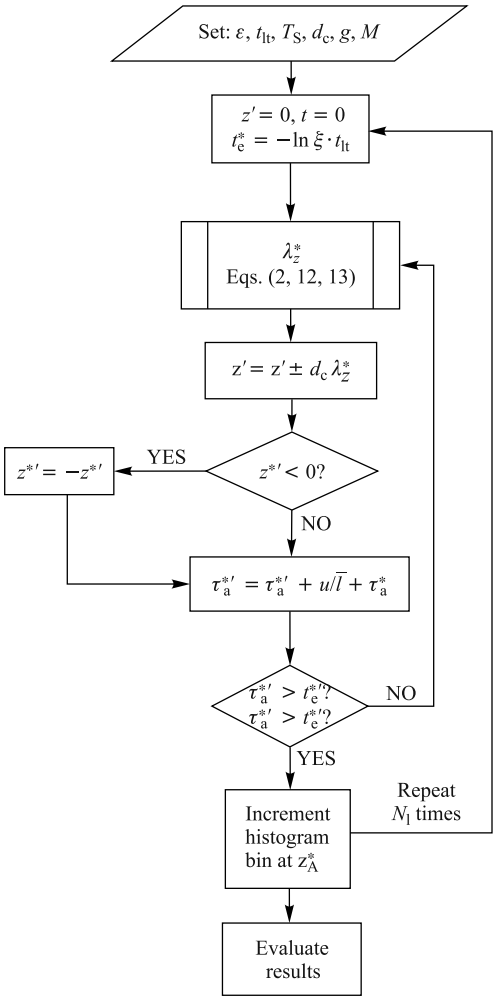

Fig. 3. A basic flow chart for the MC simulation of VTC peaks in the case of short-lived label, $t_{\rm lt} \ll t_e$. See the above list for the symbols

In practice, each of the involved molecules may have its own actual duration of the experiment; it is the case with the short-lived radiolabels due to their random lifetimes. For the possible variants and details see [1]. Here and below, if not mentioned otherwise, we deal with the case $t_{\rm lt} \ll t_e$. Notice, that any "short" in the text below emphasizes namely this condition. Consistently, we use "long" for the opposite, $t_{\rm lt} \gg t_e$.

The simplified flow chart shown in Fig. 3 is self-explanatory. The displacements yielding a negative coordinate are "reflected" at zero. When the total adsorption residence time equals or exceeds the individual $t^*_{\rm lt}$, the simulation is terminated. The small contribution of the time of flight is approximated by taking its mean, rather than random, value at the local T_z, The histogram bin corresponding to this random final z^*_A is incremented. The following data were obtained for several varieties of experimental conditions using unabridged flow charts:

$z_A = \sum_{i=1}^{N_h} z^*_{Ai}/N_h$ — weighted mean coordinate, 1st initial moment, of the peak profile, (cm),

$\overline{z^2_A} = \sum_{i=1}^{N_h} z^{*2}_{Ai}/N_h$ — 2nd initial moment of the peak profile (cm^2),

$\sigma^2_z = \overline{z^2_A} - z^2_A$ – dispersion of the peak profile (cm^2),

T_A — column temperature at z_A (K),

$\rho(z^*)$ — normalized *histogram* of the peak profile (cm^{-1}),

N_l — average number of the steps (calls for λ^*_z) in a molecular history,

N_b — average number of returns to start with reflection (the $z^{*'} \le 0$ events).

PROFILES OF VTC PEAKS AT VARIOUS EXPERIMENTAL CONDITIONS

When systematically exploring VTC chromatograms, we arbitrarily chose a *"standard" set of the experimental conditions*, which hold below if not otherwise stated; these are : $\varepsilon = 6500$ K, $T_{\rm S} = 300$ K, $g = 3$ K/cm, $d = 1$ cm, $M = 300$, the *label is short-lived* with $t_{\rm lf} = 5$ s. The corresponding peak is regarded like a sort of reference. Figure 4 and Table 2 present some characteristic data for the corresponding standard," peak plus the results for the *long-lived label* at $t_e = 5$ s and some very different durations of the experiment.

In the case of simple (constant step length) random walks, the average number of the walks is the squared average distance measured in the steps. The effective mean for variable steps is $d_c\sqrt{\overline{\lambda^2_z}}$ (see Part 2); in the present case it is $0.816 d_c$ (cf. Table 1). Table 2 shows that our $N_l \approx (z_A/0.816 d_c)^2$ is close enough to what would be with simple walks. We also counted the events which gave $z' < 0$ and so were reflected; thus we obtained the average number of the "returns to

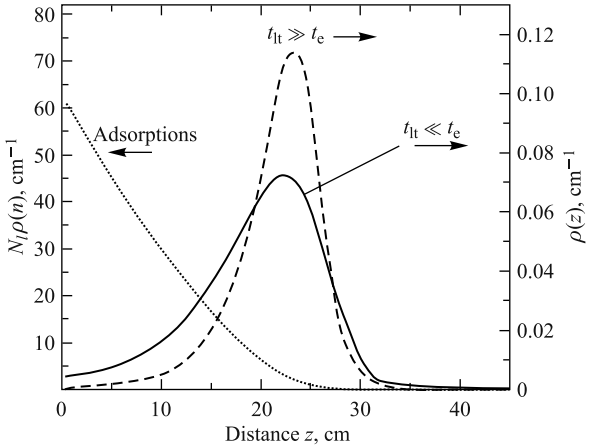

Fig. 4. The standard peak and that from the elution experiment with long (stable) label lasting 5 s (right scale); the average number of reversible adsorption events per cm (left scale); see text and N_l values in Table 2

Table 2. Statistical characteristics of the peaks for the long-lived nuclides at several durations of the experiment compared with those at the standard experimental parameters

t_e, s	T_A, K	z_A, cm	σ_z^2, cm^2	MC	$N_l(z_A/0.816d_c)^2$	N_b MC
Standard (short) label						
$t_{lt} = 5$ s	242	19.3	42	635	560	16
Long label						
0.05	281	6.2	13	79	53	5.4
5	259	13.7	28	301	280	11
5	236	21.5	29	755	695	18
50	214	28.4	21	1250	1210	22

origin"; this problem has not yet been exactly solved in mathematics even for the simple random walks. Next, we counted the average total number of the adsorption events, which took place in the standard and long-label cases, and their distribution (per cm) along the paths. That in Fig. 4 is for the short-lived molecules, with the average 650 events per molecule (the area under the curve). Meanwhile, the long-lived molecules experienced some 750 collisions, while the two distributions differ insignificantly when normalized.

Figure 5 gives a notion of dependence of the migration distance, dispersion of the profile, and detailed peak shape on some experimental conditions; cf. similar simulations of GTC in [24]. Notice that z_A and σ_z^2 strongly increase with smaller

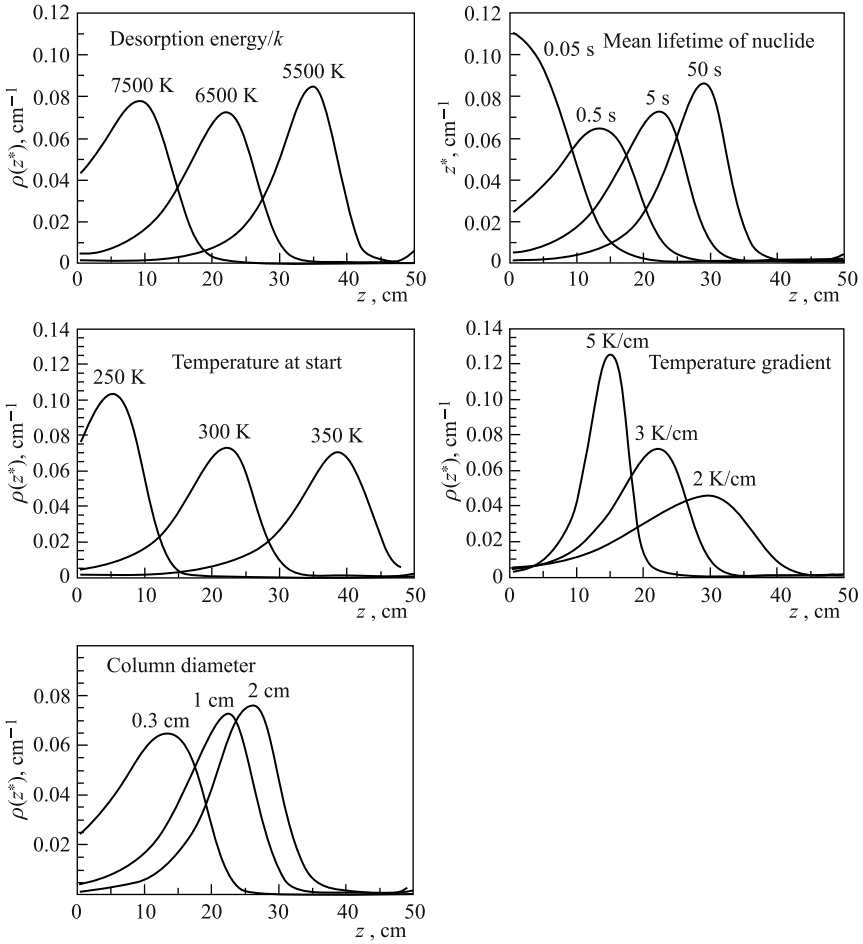

Fig. 5. The peak profiles when changing just one of the otherwise standard experimental conditions

g; larger d_c enlarges z_A but only slightly changes σ_z^2; longer t_e results in larger z_A and gradually smaller σ_z^2 dispersion; higher T_S leads to higher z_A, while T_A and σ_z^2 stay almost unaffected.

SIMPLIFIED MC SIMULATIONS

We examined the possibility of avoiding simulation of the random adsorption residence times and desorption angles by using the coordinate, and so temperature dependent τ_a, and the effective mean step lengths Δz. The latter must be the

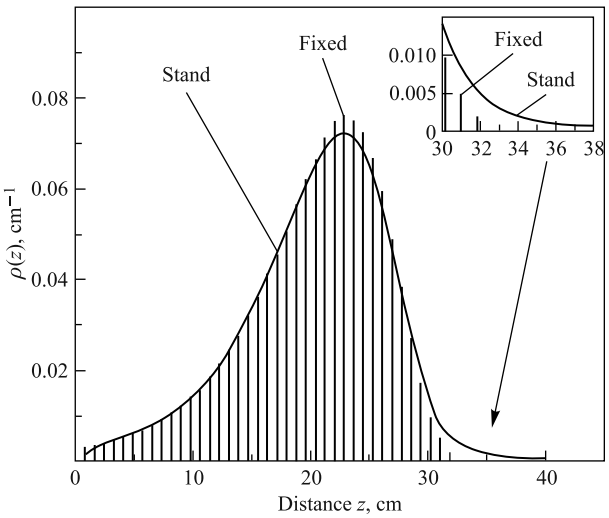

Fig. 6. The peak profiles from the standard and simplified flow charts: the insert shows magnified region of large distances; see text for details. The histogram has 0.816 cm bins

Table 3. Statistical characteristics of the peaks obtained with simplified simulation flow charts

Conditions		$\bar{z}$, cm	$\overline{z^2}$, cm^2	σ_z^2, cm^2	N_l
Standard; see flow chart in Fig. 3		18.1	356	27.3	549
Standard, but that	$\tau_a^* \equiv \bar{\tau}_a$	18.1	358	29.7	544
	$l_z^* \equiv \Delta z$	18.1	394	22.4	524
	$l_z^* \equiv \Delta z,\ \tau_a^* \equiv \bar{\tau}_a$	18.0	394	22.4	526

above-mentioned $0.816 d_c$. The simulations were done for the three possible simplifying combinations: $\lambda_z^* d_c$ with $\tau_a(z)$; Δz with $\tau_a^*(z)$; and Δz with $\tau_a(z)$. Some of the results are presented in Fig. 6 and in Table 3. The standard peak and that for $\bar{\lambda}_z^* d_c$ plus $\tau_a(z)$ practically coincide; the same takes place for Δz plus $\tau_a^*(z)$ and Δz plus $\tau_a^*(z)$. For that reason, only one representative from each pair is displayed in Fig. 6. The insert in the figure shows that with fixed Δz, the peak tail decreases more rapidly than that of the standard, because some random steps are much longer than Δz.

The considerably faster simplified simulations may seem attractive. However, for the fixed Δz, the resulting probability mass function with its $0.8165 d_c$ bins can reasonably serve the analysis of experimental data only when the longitudinal extensions of the detectors equal that bin.

COMMENTS AND CONCLUSIONS

Advantages and Disadvantages of Monte Carlo Simulations. The principle *disadvantage* of the MC approach is the impossibility of finding the functional relations between the parameters of the simulated profiles and the experimental conditions. Also the computation time is relatively long, even for the cylindrical columns, where all the free flights start in identical geometry. Moreover, to date, the experiments with heavy elements have been done with the columns of the rectangular section, which lack the site equivalence. It would require much more tedious simulations because of the lack of the site equivalence and has not yet been done. In Part 2 will be presented somewhat imperfect solution to the problem by using effective random step lengths which depend on the cross-section geometry.

The great *advantage* of the MC approach is its inherent capability of accounting for numerous realistic experimental conditions, more complicated than those assumed above. For example, in practice, it is not easy to realize the constant negative temperature gradient. Mere placing the column into an insulated metallic tubular casing, whose ends are kept at different temperatures, fails, because the thermal insulation cannot be ideal. Meanwhile, any column temperature profiles described by a function, but also by an interpolated table, etc., can be handled by MC. Easily treated can be also a column consisting of parts with dissimilar surfaces and so with suddenly changing ε. For example, very often, a low-ε isothermal initial part serves to rapidly supply the analytes to the higher ε, true VTC section.

The flow chart in Fig. 3 directly and rapidly solves the problem of short-lived labels through replacing, once per history, the nominal t_e by a random lifetime. In addition, also an eventual heterogeneity of the column surface and other complex phenomena will require just few more steps in the simplest flow chart in Fig. 3. This way one might efficiently replace the alternative straightforward approaches. For the short t_{lt}, it would mean making a large number of simulations for long t_{lt} at t_e values within a range of several t_{lt}s, followed by summation of these profiles with the weights $\exp\left(-t_e/t_{\mathrm{lt}}\right)/t_{\mathrm{lt}}$.

The width of a VTC peak usually makes a considerable fraction of the migration distance. Figure 5 evidences that managing of this disadvantage is not easy. Thus, the technique is not an omnipotent separation tool; however, it can well solve nontrivial problems. In particular, an inherent capability of VTC is to keep the column surfaces very clean and unchanged during the experiment. This is difficult to achieve in GTS because the carrier gas (maybe, otherwise inert) necessarily contains some unaccounted for impurities and intentionally added reagents. The latter are to secure the required chemical state of the analyte, but might also modify the surface in a poorly predictable way.

Closer inspection of the flow chart in Fig. 3 reveals that the simulation for some particular conditions actually provides also a plethora of generic data. In-

deed, multiplication of ε, T_S, and gd_c by a constant factor while preserving $t_{\rm lt}$does not change the chromatogram. Hence, with a factor larger than unity one obtains the chromatograms for the region of less volatile species.

Prospects for Measurement of the Desorption Energies. The thermodynamic approach to evaluating the enthalpy of desorption is evidently inapplicable if just one experiment has been done, even with good statistics. Then the only way may be to simulate the peaks for different values of ε_d and to find empirically the "best fit" to the data. The resulting ε_d depends on the accepted value of τ_0, taken as about 10^{-13}s, independent of temperature. The value comes from the vibration frequencies of the adsorbent crystalline lattice [25] and must be valid at least for physical adsorption. Alternatively, one can refer to the Eyring's "dynamic theory" [26] —.this approach via an activated complex and its thermodynamic characteristics [27] yields the same order of τ_0, but now is depending on temperature: $\tau_0 = h/kT$. Beyond doubt, both the VTC and GTC techniques exploit the localized adsorption concept. The widely used Langmuir isotherm is based on this model [28] because the mobile adsorption occurs very seldom. Indeed, in vacuum, the adsorbate as the rarefied two-dimensional gas would momentously exit the column at any temperature. On the other end, some lateral diffusion during the adsorption residence time can never be excluded, especially when — and because of — the real surfaces are heterogeneous [29]. This is why dealing with the microscopic picture, we speak about desorption rather than adsorption.

In the one-atom-at-a-time studies of the newest heavy elements, the experimental "peak" mostly consists of just a few decay events. The individual lifetimes behind the decays are unknown and the linear coordinates of the events have accuracy like 1 cm — the size of the common, position nonsensitive, detectors. Solution to the problem of the confidence interval for ε_d would be greatly enhanced if there were an explicit formula describing the peak profile as a function of the experimental parameters. MC simulations do not show a way to this goal; indeed, one can reasonably fit the simulated profiles by a peaking function, however, the parameters of the fits cannot be related to the variables.

The rigorous Monte Carlo simulations require relatively long computation time. The simplified simulations are considerably faster, but must be used carefully. For example, the "probability mass function" with a bin of $0.8165d_c$ might not allow accurate accounting for the likelihood that the detected particle actually originated on the surface of a neighboring detector.

An explicit formula for the peak would greatly enhance the otherwise tedious procedures of probabilistic evaluation of the poor statistics data. For example, the Bayesian approach would benefit from easy calculation of the likelihood of the observed data for a number of ε_d's. In a following paper, starting with the diffusion ansatz of random walks to describe the VTC chromatograms, we finally derived a semitheoretical formula for the peak profiles, which closely

approximates the MC simulations and explicitly shows the functional dependence on all basic variables. Bayesian evaluation of sample data using the formula will be presented in some details.

Acknowledgements. The author acknowledges support of this research by a grant of Plenipotentiary of Czech Republic to JINR.

REFERENCES

1. *Zvara I.* // J. Radioanal. Nucl. Chem. 2010. V. 286, P. 597–602.
2. *Steckelmacher W.* // Rep. Prog. Phys. 1986. V. 49 P. 1083–1107.
3. *Clausing P.* // Ann. Phys. (Lpz) 1930. V. 7 P. 489–568.
4. *de Boer J. H.* The Dynamical Character of Adsorption. Oxford: Clarendon Press, 1953.
5. *Feller W.* An Introduction to Probability Theory and Its Applications, 3rd ed. New York: Wiley, 1970.
6. *Westgaard L., Rudstam G., Jonsson O. C.* // J. Inorg. Nucl. Chem. 1969. V. 31. P. 3747–3758.
7. *Grappengiesser B., Rudstam G.* // Radiochim. Acta. 1973. V. 20. P. 85–96.
8. *Rudstam G., Grappengiesser B.* // Radiochim. Acta. 1973. V. 20. P. 97–102.
9. *Beyer G. J., Novgorodov A. F.* JINR Commun. P6-9917. Dubna, 1987; Report HL CERN-EP/87-172. Geneva.
10. *Gggeler H. W. et al.* // Radiochim. Acta. 1986. V. 40. P. 137–143.
11. *Eichler R., Schdel M. J.* // J. Phys. Chem. B. 2002. V. 106, P. 5413–5420.
12. *Hohn A., Eichler R., Eichler B.* // Radiochim. Acta. 2004. V. 92. P. 513–516.
13. *Davis D. H.* // J. Appl. Phys. 1960. V. 31. P. 1169–1176.
14. *Fenter F. F., Caloz F., Rossi M. J.* // Rev. Sci. Instrum. 1997. V. 68, P. 3180–3186.
15. *Eichler B., Eichler R.* The Chemistry of Superheavy Elements / Ed. M. Schödel. Dordrecht, Kluwer, 2003.
16. *Zvara I.* The Inorganic Radiochemistry of Heavy Elements — Methods for Studying Gaseous Compounds. Springer, 2008.
17. *Wenaas E. J.* // J. Chem. Phys. 1971. V. 54, P. 376–388.
18. *Miller S. L.* // Found. Phys. 2007. V. 37. P. 1660–1684.
19. *Celestini F., Mortessagne F.* // Phys. Rev. E. 2008. V. 77. P. 021202.
20. *Feres R., Yablonsky G.* // Chem. Eng. Sci. 2004. V. 59. P. 1541–1556.
21. *Prata J.* // Radiat. Phys. Chem. 2003. V. 66. P. 387–395.
22. *Yermakov S. M., Mikhailov G. A.* Statisticheskoye Modelirovanye (Statistical Modeling). M.: Nauka, 1982.
23. *Greenwood J.* // Vacuum. 2002. V. 67. P. 217–222.
24. *Erdis P., Taylor S. J.* // Acta. Sci. Hung. 1960. V. 11. P. 137–162.
25. *Frenkel J.* // Z. Phys. 1924. V. 26. P. 117–138.
26. *Felinger A.* // J. Chromatogr. A. 2008. V. 1184. P. 20–41.
27. *Laidler K. J., Glasstone S., Eyring H.* // J. Chem. Phys. 1940. V. 8. P. 659-667.
28. *Hill T. L.* // J. Chem. Phys. 1949. V. 17. P. 762–7719.
29. *Stallons J. M., Inglesia E.* // Chem. Eng. Sci. 2001. V. 56. P. 4205–4216.

Received on January 10, 2014.

Редактор *Э. В. Ивашкевич*

Подписано в печать 6.03.2014.
Формат 60 × 90/16. Бумага офсетная. Печать офсетная.
Усл. печ. л. 1,12. Уч.-изд. л. 1,57. Тираж 225 экз. Заказ № 58204.

Издательский отдел Объединенного института ядерных исследований
141980, г. Дубна, Московская обл., ул. Жолио-Кюри, 6.
E-mail: publish@jinr.ru
www.jinr.ru/publish/